CHEMICAL ENGINEERING TRANSACTIONS Volume 17, 2009
Editor Sauro Pierucci
 ISBN 978-88-95608-01-3 ISSN 1974-9791
DOI: 10.3303/CET0917125

Towards a Rigorous Solution of Population Balance Equations for the Gas Antisolvent Crystallization (GAS) Process

Yousef Bakhbakhi

Department of Chemical Engineering, King Saud University, P.O. Box 800, Riyadh 11421, Saudi Arabia. Email: ybakhbak@ksu.edu.sa

The utilization of SCFs for the processing of several products has attracted considerable interest in recent years as an emerging "green" technology. Particle formation using SCFs can be carried out according to several different techniques, including antisolvent techniques such as the gas-antisolvent (GAS) process. The potential advantages of the GAS crystallization process lies in the possibility of obtaining solvent free, micron and submicron particles with a narrow size distribution. By varying the process parameters, the particle size, size distribution and morphology can be "tuned" to produce a product with desirable qualities. However, depending on the considered particle formation mechanism, population balance model of GAS process may include phenomena such as primary nucleation, secondary nucleation, crystal growth, as well as agglomeration and/or breakage (attrition) of crystals. The resulting equation is often of the integro-partial differential form. A powerful numerical algorithm for the treatment of the implemented population balance model structures was applied in this work. Algorithm simulations were performed for changes in the main GAS process operating parameters, i.e., the antisolvent addition rate and saturation level.

KEYWORDS: population balance, crystallization kinetics, numerical algorithm, GAS.

1. Mathematical Framework

The mathematical modeling of the GAS process is a necessary step in order to achieve a fundamental understanding of the crystallization mechanisms governing this unconventional crystallization technique, and how nucleation (primary and secondary), and growth occur during the expansion process, and how this affects particle size and size distribution. Thus, the developed model has to describe the elementary physical phenomena involved in the GAS process and to relate the volumetric expansion of the liquid phase to the dynamics of particle formation. A proposed model by Muhrer et. al., 2002, was employed to fill the gap between the experimental results obtained from the GAS crystallization of phenanthrene from toluene using CO_2 as antisolvent, and the theoretical understanding of the particles formation mechanisms and the influence of the process parameters in the GAS process. The equation for a semibatch crystallizer, in

Please cite this article as: Bakhbakhi Y., (2009), Towards a solution of population balance equations for the gas antisolvent crystallization (gas) process, Chemical Engineering Transactions, 17, 747-752 DOI: 10.3303/CET0917125

which particle agglomeration and breakage are not included, and particle shapes are uniform, and size-independent growth rate is given as:

$$\frac{\partial n}{\partial t} + G\frac{\partial n}{\partial L} + \frac{n}{N_L v_L}\frac{d(N_L v_L)}{dt} = 0 \quad (1)$$

where $'n'$ represents the population density of the crystals at time $'t'$ of a given size $'L'$ per unit mass of solvent per unit size, G represents the growth rate of particles, and N_L is the molar hold-up of the liquid phase in the crystallizer.

2. Discretization Algorithm

The combination of Lax-Wendroff and Crank-Nicholson methods produces a highly efficient numerical algorithm of a finite-element type with time discretisation that leads to a stationary partial differential equation. Bennett and Rohani, 2001, have shown that while both the Lax-Wendroff and Crank-Nicholson algorithms work well for crystallization systems with smooth population balance functions, they fail when a discontinuous population density develops. To overcome this hurdle, the authors combined the Lax-Wendroff and Crank-Nicholson methods. The implementation of the combined algorithm requires the finite representation of the differential equations, which is accomplished through the construction of a Jacobi Matrix, representing the finite version.

3. Simulation

The combined method was implemented in a in a dynamic simulation program especially suited for the GAS process units. The simulations were executed for the GAS crystallization of phenanthrene from toluene, as a model system, using CO_2 as the antisolvent. The process temperature was kept constant at 25^{o}C for all of the simulations. The antisolvent addition rate, Q_A, was varied between 1 and 100 ml/min. The initial solute concentration was varied between 25% and 100% of the concentration ratio. The concentration ratio was defined as the ratio between the actual concentration of the liquid solution and the saturation concentration. The final pressure, where the antisolvent addition was terminated, is 60 bar.

4. Results and Discussion

A systematic investigation of the influence of the key GAS process parameters, antisolvent addition rate, temperature, solute concentration, and agitation rate on the particle morphology, size, and size distribution was previously performed by Bakhbakhi et. al, 2005. These experimental data were used in this work in order to achieve a qualitative comparison with the simulated results and to further confirm the accuracy of the numerical algorithm and model reliability. The secondary nucleation rate effectiveness factor, α'', was estimated within the investigated level of antisolvent

addition rate of 1 ml/min, and as presented in Table 1, was found to be in the range of $6.49*10^{-17}$. However, α'' was the only parameter controlling the qualitative effect of the process variables on the particle size, and size distribution of the final precipitate

Table 1. Simulation Results (parameter estimates).

parameter	estimated value
α''	$6.49*10^{-17}$
k_g	$5.18*10^{-5}$ m/s
g	1.69

Figures 1 and 2 show the measured versus simulated volume percent particle size distributions, as a function of the antisolvent addition rate, 100, 50, 20 and 1ml/min (100% solute concentration ratio). It is evident that the simulated particle size distribution is in a reasonable agreement with experimental data. However, small differences can be observed. The difference between associated plots could be due to the simulation assumptions such as the absence of breakage and agglomeration. At 100 ml/min addition rate, the maximum primary nucleation rate, B', attained a higher order of magnitude of $9.2*10^{12}$ than $1.3*10^{9}$ #/m^{3}s for the secondary nucleation rate, B''. The observed behaviour can be explained by the fact that at this level of addition rates, primary nucleation is much faster than secondary nucleation, whose contribution to the final unimodal particle size distribution is far smaller. It is obvious that the primary nucleation rate is more responsive to the antisolvent addition rate than the secondary nucleation rate. On the contrary at a low antisolvent addition rate of 1 and 20 ml/min, primary nucleation had a lesser effect. In these cases, secondary nucleation reaches higher rates than primary nucleation and thus, has a larger role in determining the final shape of the particle size distribution. At these levels of the antisolvent addition rate, the maximum secondary nucleation rate, B'', attained a higher order of magnitudes of $6.2*10^{6}$ than $7.9*10^{5}$ #/m^{3}s for the primary nucleation rate, B' for 1 ml/min and of $0.4*10^{8}$ than $1.4*10^{7}$ #/m^{3}s for the primary nucleation rate, B' for 20 ml/min. Thus, the primary nucleation burst forms enough particles and enough surface area to trigger secondary nucleation, whose rate under these conditions is large enough that the secondary nucleation burst forms much more particles than the primary one. As a consequence, the final particle size distribution is distinctively bimodal, as shown in Figure 2. Figure 1 illustrates also the typical behaviour at the intermediate level of antisolvent addition rate of 50 ml/min. The difference between the maximum values attained for both primary and secondary nucleation rates at this level of antisolvent addition rate, is far less in comparison to the higher addition rate, (i.e., 100 ml/min). Figure 3 shows the comparisons between the measured and simulated volume percent particle size distributions at 25 and 75 % solute concentration ratio (50 ml/min antisolvent addition rate). On the other hand, the comparisons between the measured and simulated volume percent particle size distributions at 50 and 100 % solute concentration ratio (50 ml/min antisolvent addition rate) are displayed in Figure 4.

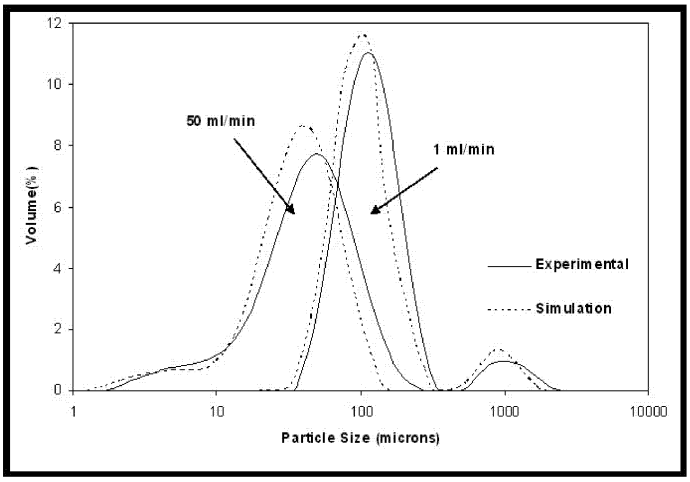

Figure 1. *Comparison between the experimental and simulated volume percent particle size distributions at the antisolvent addition rate of 1 and 50 ml/min. The antisolvent addition rates are indicated by an arrow for the experimental and simulation results (T = 25 °C, concentration ratio = 100%).*

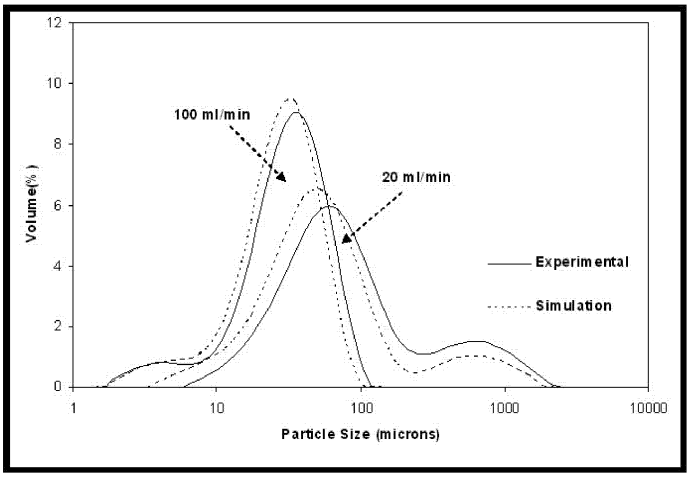

Figure 2. *Comparison between the experimental and simulated volume percent particle size distributions at the antisolvent addition rate of 20 and 100 ml/min. The antisolvent addition rates are indicated by an arrow for the experimental and simulation results (T = 25 °C, concentration ratio = 100%).*

It is evident that the predicted and experimental particle size distributions are in a good agreement. However, small inconsistencies can be noticed. At 25 % solute concentration ratio, the maximum primary nucleation rate, B', attained a higher order

of magnitude of $1.55*10^{12}$ than $0.90*10^{9}$ #/m^{3}s for the secondary nucleation rate, B'', whose contribution to the final unimodal particle size distribution is far smaller.

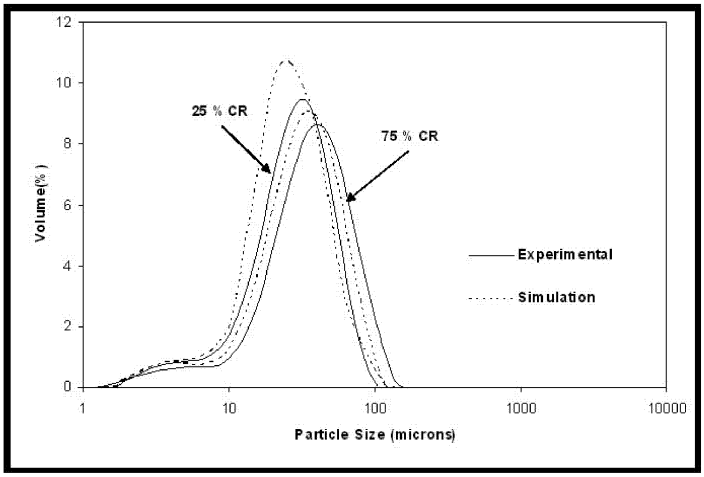

Figure 3. *Comparison between the experimental and simulated volume percent particle size distributions at 25% and 75% solute concentration ratios. The solute concentration ratios are indicated by an arrow for the experimental and simulation results (T = 25 °C, antisolvent addition rate = 50 ml/min).*

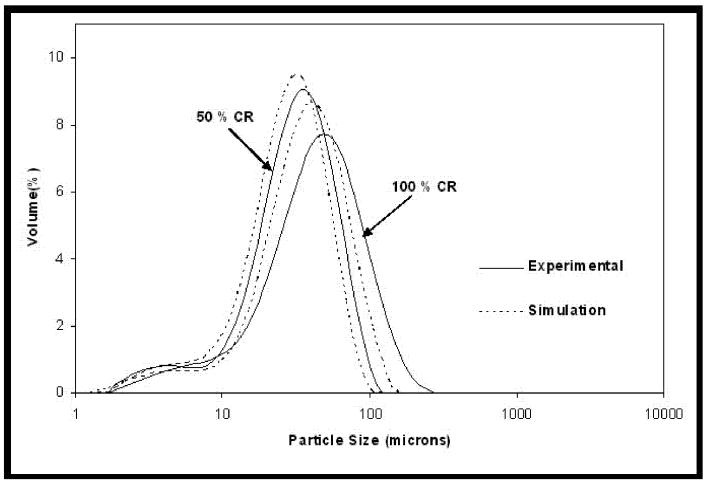

Figure 4. *Comparison between the experimental and simulated volume percent particle size distributions at 50% and 100% solute concentration ratios. The solute concentration ratios are indicated by an arrow for the experimental and simulation results (T = 25 °C, antisolvent addition rate = 50 ml/min).*

It is evident that the primary nucleation rate is less responsive to the initial solute concentration than the secondary nucleation rate, as the maximum primary nucleation rate attained a lower order of magnitudes of $2.0*10^{11}$, $6.1*10^{10}$, and $5.5*10^{10}$ #/m^3s at 50, 75, and 100% solute concentration ratio, respectively.
The exhibited behaviour can be explained by considering that, during volume expansion at higher solute concentrations, the supersaturation profile tends to get quickly closer to the saturation line initiating a primary nucleation burst, and thus, longer time for the particles formed during the first burst of nucleation to grow, i.e., the growth mode dominates and superimposes to secondary nucleation, and thus, larger size particles with broad particle size distribution are generated.
Evidently, the e algorithm produced a stable and smooth solution that tackled the complex population balance structures of the GAS process rather successfully. The dynamic behaviour of the combined method has turned out to be a very stable and reliable one, in particular for moving particle size distributions, with no observable oscillations or uncertainty.

5. Conclusions

The combined numerical algorithm was successfully able to treat the implemented population balance model structures, producing smooth dynamic and steady state particle size distributions. Moreover, the simulation results were consistent with the experimental results, and reasonable agreement was achieved.

Acknowledgments

The author wish to acknowledge the financial support by Deanship of Scientific Research at the King Saud University.

References

Bakhbakhi, Y.; Rohani S.; Charpentier P., 2005, Micronization of Phenanthrene Using the Gas Antisolvent Process.1. Experimental Study and Use of FTIR. *Ind. Eng. Chem. Res.*, 44, 7337-7344.

Bennett, M. K.; Rohani S., 2001, Solution of population balance equations with a new combined Lax-Wendroff/Crank-Nicholson method. *Chem. Eng. Sci.*, *56*, 6623-6633.

Hounslow, M. J., 1990 A Discretized population balance for continuous systems at steady state. *AIChE Journal*, 36(1), 106–116.

Hounslow, M. J.; Ryall, R. L.; Marshall, V. R., 1988, A discretized population balance for nucleation, growth, and aggregation. *AIChE Journal*, 34(11), 1821–1835.

Muhrer, G.; Lin, C.; Mazzotti, M., 2002, Modeling the gas antisolvent recrystallization process. *Ind Eng Chem Res.*, 41, 3566-3579.

Randolph, A.; Larson, M. A., 1988, *Theory of particulate processes, 2nd edition.* Academic Press, Inc.: San Diego, CA.